End-to-End Diffusion Coefficients and Distance Distributions from Fluorescence Energy Transfer Measurements: Enhanced Resolution by Using Multiple Donors with Different Lifetimes

Ignacy Gryczynski,[1] Joseph R. Lakowicz,[1] and Józef Kuśba[1]

We describe a method to improve the resolution of donor-to-acceptor distance distributions in molecules which are flexing on the timescale of the fluorescence lifetime. We measured the time-dependent donor decays of two donor (D)–acceptor (A) pairs, where the donor lifetimes were substantially different. The donors were an indole residue (5.7 ns) and a naphthalene residue (24.4 ns). The same dansyl acceptor was used for both D-A pairs. The donor decays are complex due to both a distribution of D-A distances and D-A diffusion. Using the donor decay data for each D-A pair alone, it is difficult to resolve both the distance distribution and the D-to-A diffusion coefficient. However, these values are unambiguously recovered from global analysis of the data from both D-A pairs. The increased resolution from the global analysis is apparently the result of the complementary information content of the data for each D-A pair. The shorter-lived indole donor provides more information on the time-zero distance distribution because there is less time for D-A diffusion, and the longer-lived naphthyl donor is quenched to a greater extent than indole due to the longer time for diffusion-enhanced energy transfer. Simulations were also used to demonstrate the increased resolution of global analysis with different lifetime donors to obtain distance distribution parameters in the presence of D-A diffusion.

KEY WORDS: Diffusion coefficients; energy transfer; multiple donors; distance distributions.

INTRODUCTION

There is considerable interest in the flexibility and conformational dynamics of complex molecules and their role in the function of biological macromolecules [1,2]. Fluorescence methods have found widespread applications in studies of conformational dynamics. For instance, fluorescence anisotropy measurements have been widely used to observe internal flexibility of proteins, membranes, and other biological assemblies [3–5]. Similarly, fluorescence resonance energy transfer (FRET)

measurements have found wide-ranging applications as a spectroscopic ruler due to its dependence on the distance between the donor and the acceptor molecules [6–9]. In the case of a flexible molecule, however, there exists a range of distances rather than a unique distance between the fluorophores. In this case resolution of the distance distribution requires high-resolution measurements of the donor decay [10,11]. Resolution of the distance distribution becomes even more complex and difficult in the presence of donor (D)-to-acceptor (A) diffusion [12,13], as can be expected to occur for peptides, proteins, and nearly all macromolecules. In fact, some authors have claimed that such resolution is not possible, based on simulated time-domain measurements of the donor decays [14]. However, experimental fre-

[1] Center for Fluorescence Spectroscopy, Department of Biological Chemistry, University of Maryland School of Medicine, 108 North Greene Street, Baltimore, Maryland 21201.

quency-domain measurements have accomplished this task [11,13,15].

These considerations of distance-distributions measurements reflect the fact that it is difficult to resolve multiexponential and/or distribution functions from measurements of time-resolved fluorescence. Therefore, it is of considerable importance to devise better methods to obtain increased resolution of these parameters. One way to reduce significantly cross correlation among the distance distribution parameters, and to improve their resolution, is to link some of the parameters in a model-dependent way often called global analysis [16]. In FRET measurements of distance distributions in the presence of diffusion, the variables which can be linked across different sets of experimental data are the distance distribution and/or rate of diffusion. In our earlier experiments we assessed the improved resolution which can be obtained by such global analyses [17–20]. We observed moderate improvement by changing the diffusion coefficient by a factor of 50 with the assumption that the distance distribution was the same at high and low viscosity [17]. Significantly enhanced resolution was also achieved by reducion of the donor lifetime (and Förster distance) using an external quencher, followed by global analysis. In this case we assumed that the distance distribution and diffusion coefficient were not affected by the quencher [18]. Similarly, in their simulation study [14], Beechem and Haas predicted improved resolution in the distance distribution parameters by the simultaneous analysis of both the donor and the sensitized acceptor fluorescence decays. However, they did not consider the possible loss in resolution due to directly excited acceptor fluorescence, which is always present in donor-acceptor systems and considered only time-domain measurements.

In this communication we assess the possible enhancement of resolution of the distance distribution parameters and the diffusion coefficient when the lifetime of the donor is varied by the use of multiple donors. We reasoned that a short-lived donor would have less time to diffuse and, thus, reveal mostly the distance distribution. In contrast, the longer-lived donor should be more sensitive to D-A diffusion. Since the donor decays will contain different information about the system, one can expect global analysis to decrease parameter correlation and increase resolution of the distance distribution and D-A diffusion coefficient.

MATERIALS AND METHODS

The measurements were performed in methanol at 20°C on a 10-GHz frequency-domain instrument [21].

The methanol solutions of the donor or donor–acceptor, with optical densities near 0.10, were excited at 287 nm with vertically polarized light. The emission was observed with magic angle conditions through a 340-nm Schott interference filter, 10-nm bandpass. Synthesis of the donors and donor–acceptor pairs was described previously in detail [22].

THEORY AND DATA ANALYSIS

The theory and fitting procedure have been described in considerable detail in earlier publications [17,23]. Briefly, the donor-to-acceptor probability distance distribution at the moment of excitation ($t = 0$) is assumed to be described by

$$P(r) = \frac{1}{Z} \exp\left[-\frac{(r - R_{av})^2}{2\sigma^2} \right] \qquad (1)$$

where Z is the normalization factor, R_{av} is the mean distance, and the half-width (hw) of the distribution is given by $\sigma \sqrt{8 \cdot \ln 2}$. The initial number $N_0^*(r)$ of the excited molecules with the donor-to-acceptor distance r is related to the total number of the excited molecules N_{t0}^* by the equation

$$N_0^*(r) = N_{t0}^* P(r) \qquad (2)$$

The donor and acceptor moieties are assumed to undergo mutual diffusion characterized by a diffusion coefficient D. The time-dependent change in concentration, $N^*(r,t)$, of excited donor molecules with the end-to-end distance r is described by the diffusion equation with an additional distance-dependent transfer term,

$$\frac{\partial \bar{N}^*(r, t)}{\partial t} = -\frac{1}{\tau_0}\left[1 + \left(\frac{R_0}{r}\right)^6 \right] \bar{N}^*(r, t)$$
$$+ \frac{1}{N_0^*(r)} \times \frac{\partial}{\partial r}\left[N_0^*(r) D \frac{\partial \bar{N}^*(r, t)}{\partial r} \right] \qquad (3)$$

In this expression $\bar{N}^*(r,t) = N^*(r,t)/N_0^*(r)$ is the excitation probability normalized by the $t = 0$ distance distribution, τ_0 is the donor fluorescence lifetime in the absence of an acceptor, and R_0 is the Förster distance for donor–acceptor energy transfer. At each distance r the rate ($k_T(r)$) of donor-to-acceptor transfer is $k_T(r) = \tau_0(R_0/r)^6$. To recover the donor distribution and diffusion parameters, Eq. (3) was solved with appropriate initial and boundary conditions. The resulting values of $N^*(r,t)$ were used to compute the donor intensities by the relation

$$I(t) = I_0 \int\limits_{r_{max}}^{r_{min}} P(r) \, \overline{N} * (r, \, t) \, dr \qquad (4)$$

where r_{min} and r_{max} are minimal and maximal donor-to-acceptor distances. Note that the excited state distribution $N*(r,t)$ is not necessarily equal to the ground state of $t = 0$ distribution.

The data were also fit to a multiexponential decay

$$I(t) = I_0 \sum_i \alpha_i \exp \, (-t/\tau_i) \qquad (5)$$

where α_i are the preexponential factors, $\Sigma\alpha_i = 1.0$, and τ_i the decay times. The fractional intensity (f_i) of each component in the decay is given by $f_i = \alpha_i\tau_i/\Sigma_j\alpha_j\tau_j$. The mean decay time $\langle\tau\rangle = \Sigma_i f_i\tau_i$.

The intensity decays were measured using the frequency domain method. The goodness-of-fit is characterized by

$$\chi_R^2 = \frac{1}{\nu} \sum_\omega \left[\frac{\Phi_\omega - \Phi_{c\omega}}{\delta\Phi} \right]^2$$
$$+ \frac{1}{\nu} \sum_\omega \left[\frac{m_\omega - m_{c\omega}}{\delta m} \right]^2 \qquad (6)$$

where ν is the number of degrees of freedom, and $\delta\phi$ and δm are the experimental uncertainties in the measured phase angles (ϕ_ω) and modulation (m_ω), respectively. These uncertainties were taken to be $\delta\phi = 0.2°$ and $\delta m = 0.005$.

For the global analysis with two donors the sum in Eq. (6) extends over the frequency-domain data for both D-A pairs. In this case the values of τ_0 is different in Eq. (3) for each donor and is determined from separate measurements of the donor-alone molecule under the same experimental conditions. In the global analysis the value of R_{av}, hw, and D are the same for both sets of data.

RESULTS

Emission Spectra

The chemical structures of the donor control and donor-acceptor pairs are shown in Fig. 1. Essentially the same linker joins the indole-dansyl (TU2D) and naphthalene-dansyl (NU2D) D-A pairs. The links differ by a single carbon atom, which was not found to be significant for the present measurements. The indole and naphthalene donors were chosen because we expected the lifetimes to be substantially different. The frequency-domain (FD) measurement of the donor control mole-
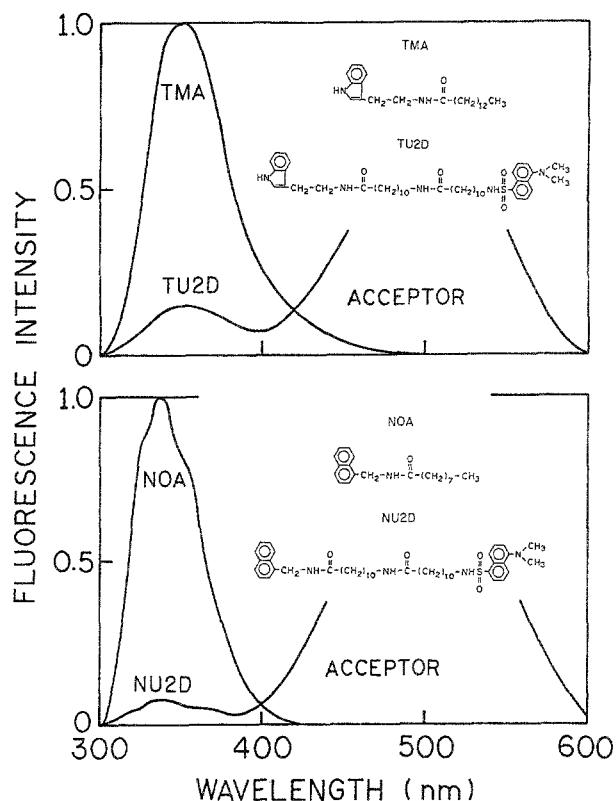

Fig. 1. Emission spectra of the two donor–acceptor pairs in methanol at 20°C. The emission spectra of the D-A pairs are shown relative to the donor-only emission spectra.

cules (not shown) revealed lifetimes of 5.7 and 24.4 ns, in air-equilibrated methanol at 20°C.

The emission spectra of the donor controls (TMA, NOA) and donor–acceptor pair (TU2D, NU2D) are shown in Fig. 1. The emission from both donors is centered at 350 nm, and the emission from the dansyl acceptor is centered at 500 nm. In our donor–acceptor pairs the linker is flexible. Consequently, there exists a variety of conformation, each with a different donor-to-acceptor distance. Additionally, donor-to-acceptor diffusion during the excited state lifetime of the donor results in the increased efficiency of energy transfer. The contribution of diffusion accounts for the increased extent of energy transfer for NU2D (Fig. 1, bottom) as compared with TU2D (top), since the Förster distances (R_0) for indole-dansyl ($R_0 = 24.9$) and naphthalene-dansyl ($R_0 = 20.9$) are similar.

The steady-state data alone provide little information on the D-to-A distance distribution and rate of D-A diffusion. (The calculated distributions can be tested for consistency with the steady-state data.) However, information on the donor-to-acceptor distance distribution

is contained in the intensity decay of the donor. This is because the distribution of donor–acceptor distances is responsible for increased heterogeneity of the donor fluorescence decay. If only one conformation (or distance) exists, then the donor will remain a single-exponential fluorescence decay, and the donor decay will only be shortened by the energy transfer process. In contrast, a range of D-A distances results in a range of transfer rates, which in turn results in a nonexponential decay of the donor. In fluid solution the donor decay becomes still more complex in its molecular interpretation. This is because the donor-to-acceptor distance distribution evolves in time due to end-to-end diffusion. If the donor displays a long decay time, then evolution of the excited state population can be significant, resulting in lost information on the initial distribution parameters (R_{av} and hw). However, the data for the longer-lived donors should contain substantial information on the D-A diffusion coefficient. In contrast, the intensity decay of a short-lived donor is expected to contain more information on initial $t = 0$ distribution since there is less time for D-A diffusion.

Simulations of the Distance-Dependent Excited-State Populations

Prior to measuring the above D-A pairs we used simulated data to reveal the effects of D-A diffusion on short- and long-lived donors. For these simulations we used distribution parameters and diffusion coefficients expected for our flexible donor–acceptor pair, in fluid solution with the linker containing about 22 methylene groups, i.e., $R_{av} = 20$ Å, hw $= 15$ Å, and $D = 10^{-5}$ cm²/s. For the long-decay time D-A pair we used $\tau_0 = 25$ ns and $R_0 = 25$ Å and for short decay time $\tau_0 = 5$ ns and $R_0 = 25$ Å. The time- and distance-dependent populations are shown in Fig. 2 for the case of a long-lifetime donor (25 ns; - - -) and a short-lifetime donor (5 ns; ——). These surfaces show that energy transfer is considerably more effective in depopulation of the donor for the long-lived sample, as is seen from the more rapid decay of the donor population. Note that the time axis is normalized to the decay time (τ_0) in the absence of energy transfer.

It is of interest to examine the time-dependent distance distributions of the excited donors. These can be seen from the distance distribution of the excited donors at $t = 0.2\tau_0$, and comparison of these distributions with the ground-state ($t = 0$) distribution (Fig. 3). The distributions (Fig. 3, left) reveal that the long-lived donor decays more rapidly than the short-lived donor, on the t/τ_0 time scale. The peak-normalized distributions (Fig.
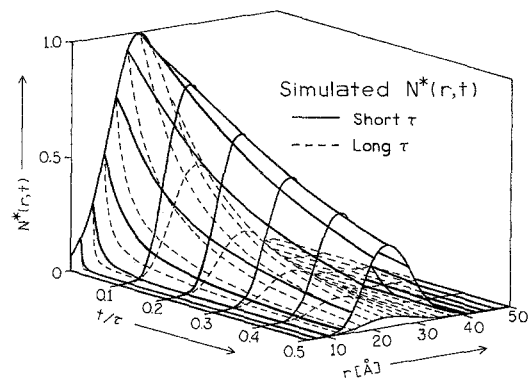

Fig. 2. Simulated time- and distance-dependent excited-state donor populations for the short-lived (——) and long-lived (- - -) donor–acceptor pairs. Note that the time axis is t/τ_0, where τ_0 is the donor decay time. The assumed donor decay times were 5 ns (——) and 25 ns (- - -). Energy transfer is more effective in depopulation of the excited donors for the long-lived donor (- - -) because of the effects of donor-to-acceptor diffusion during the excited-state lifetime.
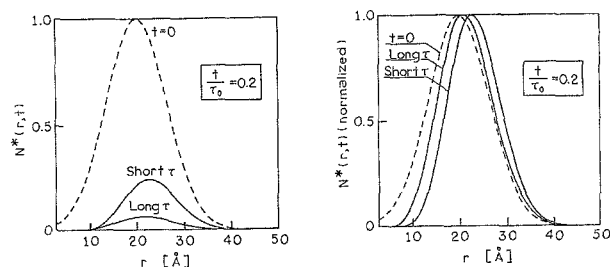

Fig. 3. Distance-dependent excited-state population at $t = 0$ and at t $= 0.2\ \tau_0$ for the 5-ns (——) and 25-ns (- - -) donors. The left panel shows the excited-state population at $t = 0$, and the populations at $t/\tau_0 = 0.2$ for the short-and long-lived donors. The right panel shows these same excited-state population peak normalized.

3, right) show that diffusion results in more closely spaced pairs than the $t = 0$ distribution. The longer-lived donor allows more time for diffusion, and hence more of these closely spaced pairs. Since these pairs are rapidly lost by energy transfer, diffusion results in an increase in the rate of transfer and a faster total donor decay.

The excited state donor populations seen in Fig. 2 can be used to predict the time-dependent donor decays. This is accomplished by integration of the distance-dependent populations over the range of allowed D-to-A distances. The intensity decays of the long and short lived D-A systems, plotted on the relative time scale t/τ_0, are shown in Fig. 4. These simulated decays clearly illustrate the increased contribution of diffusion to the donor decay kinetics for the longer lived donor. These differences in the time- and distance-dependent popula-
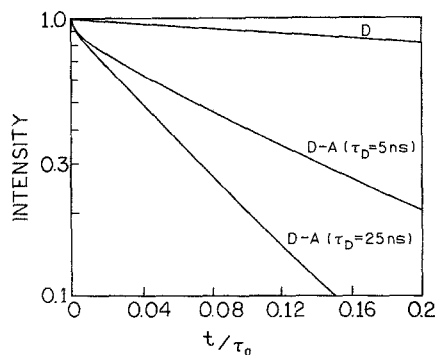
Fig. 4. Simulated intensity decays of the donor alone, and for the short- and long-lived donor–acceptor pairs. Note the relative time scale (t/τ_0).

tions (Figs. 2–4) suggest that different information is available for longer and shorter donor decay times, which should be an advantage when using global analysis of samples with different donors.

We used the time- and distance-dependent populations to calculate the frequency response of the donor emission. Phase and modulation values were calculated for 20 regularly spaced frequencies. The frequency range of the simulations was adjusted so that the highest frequency results in a modulation of about 0.15 for both the quenched and the unquenched sample. This is characteristic of our measurements, which are performed over the widest possible range of frequencies consistent with acceptable signal-to-noise ratio. The larger dots represent the simulated data. The dotted lines represent the decay of the donor in the absence of energy transfer. Hence the shift in the simulated data from the donor decays represents the reduction in mean decay time of the donor due to energy transfer. The larger frequency shift between the 25-ns donor and the simulated data illustrates the increased transfer efficiency for the longer-lived donor.

The solid lines in Fig. 5 represent the best fits to the simulated data taking into account end-to-end diffusion (D) as a floating parameter. The dashed lines show the expected frequency response if the diffusion is ignored, that is, if D is set equal to zero. The differences between the solid and dashed lines are qualitative indicators of influence of diffusion. One notices that reasonably good fits to the simulated data can be obtained with the diffusion coefficient held equal to zero ($\langle D \rangle = 0$). The values of χ_R^2 for the $\langle D \rangle = 0$ fits are elevated 3.4- and 11.2-fold for the 25- and 5-ns donors, respectively (Table I). The higher elevation in χ_R^2 is expected for the shorter-lived (5-ns) donor because there is less time for diffusion to "blur" the effects of the $t = 0$ distance
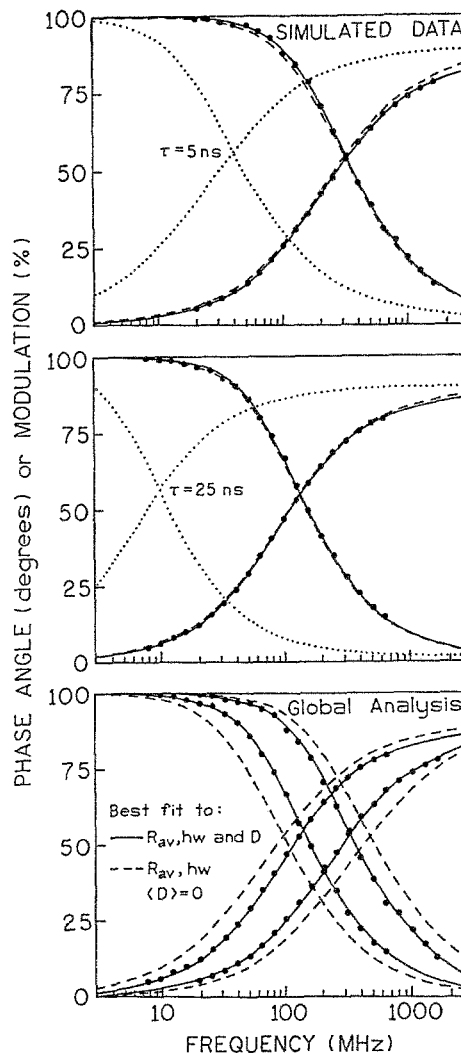

Fig. 5. Simulated frequency responses of the donor emisison for two donor–acceptor pairs. The distance distribution was assumed to be a Gaussian with $R_{av} = 20$ Å and hw $= 15$ Å [Eq. (1)], with $D = 10^{-5}$ cm²/s. The filled circles are the simulated data, and the solid lines are the best fits which include diffusion. The dashed lines show the expected frequency response if the diffusion is ignored. The dotted lines show the simulated frequency response of teh donor, without energy transfer.

distribution. While these values of χ_R^2 are adequate to detect diffusion, analysis of each D-A pair above provides only modest resolution of the distance distribution and diffusion parameters. Apparently a close fit to the data can be obtained if R_{av} and hw are allowed to vary to compensate for the absence of diffusion. Such correlation between the parameters suggests the need for additional data to recover reliably the parameter (R_{av}, hw, and D) values.

The single D-A pair and global analyses of the simulated data are summarized in Table I. We were able to

Table I. Single D-A Pair and Global Analysis of Simulated Frequency-Domain Data for Distance Distributions in the Presence of D-A Diffusion

Assumed value				Recovered value[a]			
τ (ns)	R_{av} (Å)	hw (Å)	D (cm²/s)	R_{av} (Å)	hs (Å)	D (cm²/s)	χ_R^2
5	20	15	10^{-5}	19.8 (0.2)	14.6 (0.8)	8.8×10^{-6} (1.1×10^{-6})	1.2
						$< D = 0 >$	11.2
25	20	15	10^{-5}	19.9 (0.2)	14.7 (0.2)	9.8×10^{-6} (0.6×10^{-6})	0.9
						$< D = 0 >$	3.4
5 and 25	20	15	10^{-5}	20.0 (0.1)	14.9 (0.1)	9.8×10^{-6} (0.2×10^{-6})	1.0
						$< D = 0 >$	674.8

[a]Values in parentheses or the uncertainties estimated from the least-squares analysis [24]. The angle braces indicate that the diffusion coefficient was held equal to zero for this particular analysis.

recover the expected distance distribution and diffusion coefficient using data from a single D-A pairs. However, the confidence intervals are substantial for the single-pair analyses (Table I). Additionally, if these single-pair data are analyzed with D focused equal to zero $\langle D = 0 \rangle$, then the χ_R^2 values are only marginally elevated (4- to 10-fold). This result indicates that there is considerable correlation between these parameters (R_{av}, hw, and D), as suggested previously [14]. In contrast, if both sets of data are analyzed globally with $D = 0$, then χ_R^2 is remarkably elevated (670-fold; Table I). This result is shown in Fig. 5 (lower panel). In this figure one observes that it is not possible to even approximately fit the data to the distance-distribution model [Eq. (1)] without D-A diffusion, as can be seen from the dashed lines in the lower panel.

One result of D-A diffusion is the decrease in the frequency shift between the data sets on the modulation frequency axis. If D is held fixed at zero, then there is a fixed difference between the two calculated frequency responses, which depends on the unquenched lifetime of the two donors. This frequency shift is decreased in the presence of D-A diffusion. Consequently, it is not possible for the fitting algorithm to do anything except place these diffusionless frequency responses in either side of the data (Fig. 5, lower panel). This result demonstrates that global analysis will improve the resolution of D-A diffusion because the diffusion coefficient is needed to match the difference between the frequency responses, independent of the shape of the individual responses.
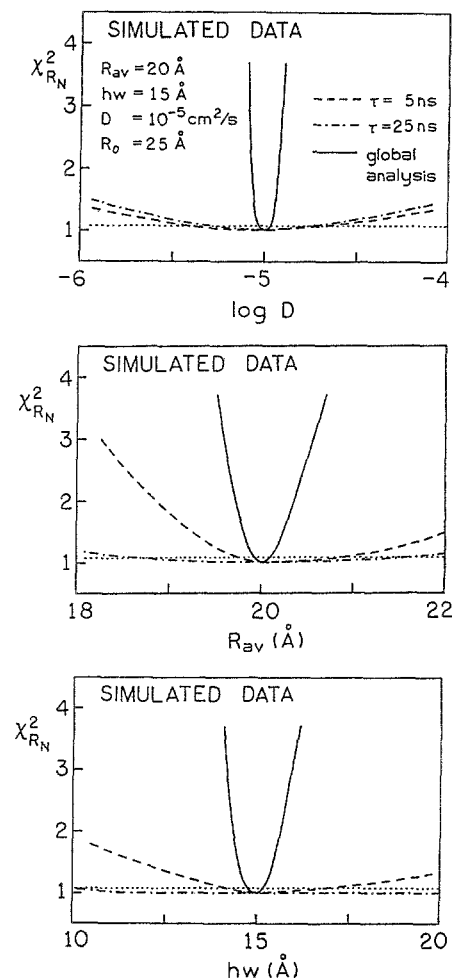

Fig. 6. The χ_R^2 surfaces for distance distribution parameters and for the diffusion coefficient (top; D in cm²/s) obtained from the simulated data. The horizontal dotted line represents the 67% confidence limit for the degree of freedom.

According to our experience, the most accurate representation of the confidence interval for each parameter is determined from the χ_R^2 surfaces (Fig. 6). We examined the values of χ_R^2 for each parameter separately by holding the parameter fixed at the values indicated on the x axis and allowing two other parameters to vary so as to minimize χ_R^2. This allows the other parameters to vary in order to minimize χ_R^2 and, hence, account for correlation between the parameters. The χ_R^2 surfaces for all three floating parameters are presented in Fig. 6. Global analysis with different lifetimes of the donor provides a significant improvement in the resolution of the distance distribution parameters as well as in diffusion coefficient. This improvement can be seen by the steep parabolic surfaces for the global analysis (———), as compared with the χ_R^2 surfaces for the single D-A
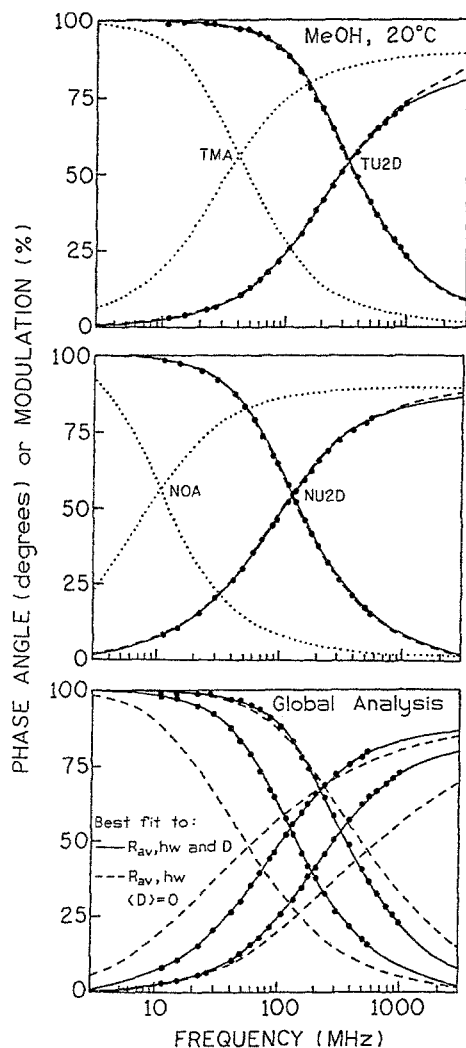
Fig. 7. Frequency response of donors and donor–acceptor pairs. The solid lines show the best distance distribution fits. The dotted lines show the frequency responses of the donors TMA (τ_0 = 5.7 ns) and NOA (τ_0 = 24.4 ns). The dashed lines show the best fits if diffusion is ignored (D = 0), but the distance distribution parameters (R_{av} and hw) are variable.

Table II. Experimental Resolution of Distance Distributions Using One or Two D-A Pairs

Sample	R_{av} (Å)	hw (Å)	D (cm²/s)	χ_R^2
TU2D[a]	19.1	18.7	1.5×10^{-5}	1.2
	(0.1)	(1.1)	(0.2×10^{-5})	
TU2D			$< D = 0 >$[c]	3.8
NU2D[b]	16.8	13.5	64×10^{-6}	2.8
	(0.9)	(2.6)	(0.1×10^{-6})	
NU2D			$< D = 0 >$	3.0
TU2D and	18.7	17.4	1.2×10^{-5}	2.3
NU2D	(0.1)	(0.1)	(0.1×10^{-5})	
			$< D = 0 >$	1918.0

[a]The decay time of TMA is a single exponential, 5.7 ns.
[b]The decay time of NOA is a single exponential, 24.4 ns.
[c]The value of D was held equal to zero for these analyses.

pairs ($- - -$, $- \cdot - \cdot -$). It is clear from these surfaces that the global analysis results in a sharper dependence of χ_R^2 on the parameter values. Hence, the use of multiple donors to vary the donor decay times is recommended for investigations of diffusion-dependent energy transfer.

Experimental Results

Frequency-domain data for the two donor–acceptor pairs (●) are shown in Fig. 7 (upper two panels). In both cases we could fit the data with recovery of the three parameters, R_{av}, hw, and D (Table II). However, reason-

ably good fits were also obtained with the diffusion co-efficient held equal to zero (Fig. 7; $- - -$), indicating that the three parameters are only weakly determined from the data. The relative χ_R^2 elevation for $\langle D = 0 \rangle$ is smaller for NU2D than for TU2D (Table II), in agreement with our expectation that a longer-lived donor provides less information about the time = 0 distance distribution.

To obtain increased resolution of the conformation and dynamics, we performed a global distance distribution analysis of the data with two different donors. A single distance distribution function is used for the least-squares analysis of both data sets for the D-A pairs. Also, the D-to-A diffusion coefficient is assumed to be the same for both D-A pairs. The solid lines in Fig. 7 (bottom) represent the best global fit to the data. The ability to fit the data with a single set of parameters support our claim (above) that the single carbon atom difference in the linker is not significant for the data, and supports our assumption that the same value of R_{av}, hw, and D describe both D-A pairs. The data could not be fit with $\langle D = 0 \rangle$, as can be seen from the lower panel in Fig. 7 ($- - -$). Examination of the lower panel in Fig. 7 shows that a nonzero diffusion coefficient is needed to account for both the shape of the individual frequency responses and the relative frequency difference between the responses. One notices that the frequency response becomes more like a single exponential in the presence of diffusion, an effect which has been observed previously [25].

We examined the uncertainties obtained from the χ_R^2 surfaces (Fig. 8). The horizontal dotted lines in Fig. 8 indicate the values of the parameters at which χ_R^2 was elevated so that there was only a 33% chance that the

increase was due to random errors in the data, for the degrees of freedom in the global analysis. It is evident that the use of two different donors results in a significantly decreased uncertainty for all parameters, particularly the end-to-end diffusion coefficient.

It is of interest to examine the range of distance distributions which are consistent with the experimental data. These distributions are shown in Fig. 9. The greatest uncertainty was observed for the NU2D (middle panel) due to its long decay time. Less uncertainty was found for TU2D (top) as expected for a shorter lived donor and less time for D-to-A diffusion. Global analysis resulted in the least uncertainty in the D-A distance distribution (bottom).

DISCUSSION

Time-resolved fluorescence intensity measurements of diffusion-dependent energy transfer, measured in the frequency domain, can provide the information necessary to recover the distance distribution parameters and end-to-end diffusion coefficients of flexible molecules. However, the resolution obtained from a single measurement can be modest and estimated values of the recovered parameters can be questionable. Beechem and Haas [14] have recently discussed this problem for time-domain measurements and suggested simultaneous analysis of the donor and acceptor decay kinetics. This type of global analysis is potentially valuable and intuitively obvious, but is very difficult to realize in practice. Usually, acceptors are excited simultaneously during the excitation of the donor, and amount of excited acceptor molecules due to energy transfer can be small compared with the whole population of excited state acceptors. That is, the population of excited acceptors can be dominantly the result of acceptors which are directly excited. The time-dependent decay of these acceptors do not contain any information on the distance distributions or dynamics, and this component can only result in decreased information content and/or decreased resolution from the data. One must also be able to observe separately the donor and acceptor emission, or introduce additional parameter into the analysis to account for emission spectral overlap. In contrast, the global analysis obtained by varying the donor lifetime does not introduce any additional parameters, gives a significant increase of the resolution for each fitted parameter, and can be used for any donor–acceptor system including nonfluorescent acceptors.

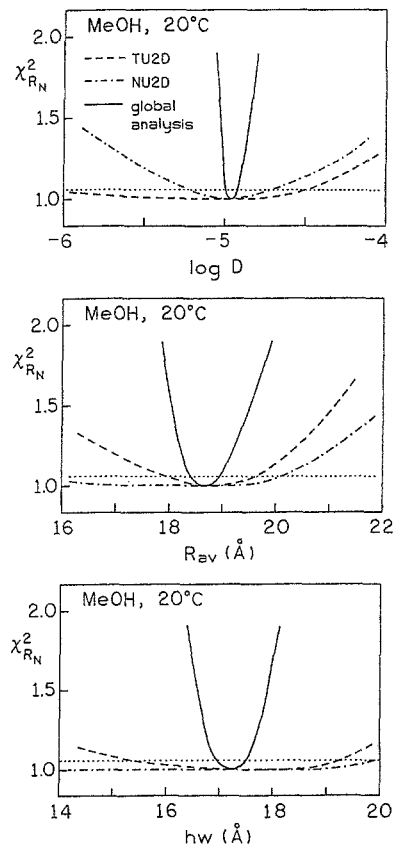The recovered initial ($t = 0$) distance distribution (Fig. 9) is in very good agreement with that found pre-

Fig. 8. Distance distribution (R_{av} and hw) χ_R^2 surfaces and diffusion coefficient (top) χ_R^2 surfaces. Also shown are the χ_R^2 surfaces for analysis of only the TU2D sample (– – –) and only the NU2D sample (– . – . –). The horizontal dotted line is for the number of degrees of freedom for the global analysis.

viously for TU2D in viscous solution [22]. The diffusion coefficient, $D \approx 10^{-5}$ cm²/s (100 Å²/ns) is in the range of expected values for small molecules in low-viscosity solutions. It is interesting to compare the end-to-end diffusion coefficient with that obtained for nonlinked system. Indole-to-dansyl intermolecular energy transfer has been investigated previously in propylene glycol and methanol [26]. The data were fitted well to a Gösele *et al.* model [27], yielding a diffusion coefficient in methanol at 20°C, $D = 2.64 \times 10^{-5}$ cm²/s. The end-to-end diffusion coefficient obtained for TU2D in methanol is only two to three times smaller than that recovered from the mixture of indole and dansyl, where the polyethylene linker was not present. The data obtained for the TU2D donor–acceptor system and indole–dansyl mixture show that the polyethylene linker containing about 20 carbons is highly flexible and has only a moderate influence on the rate of D-A.
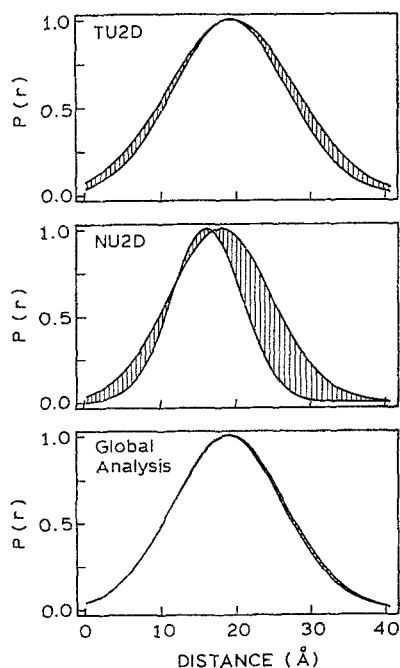
Fig. 9. Donor-to-dansyl distance distributions. The hatched area shows the range of distance distributions [Eq. (1)], which are consistent with the data for TU2D (top), NU2D (middle), and for global analysis, NU2D (bottom).

And, finally, we note that the use of donors with different decay times is potentially valuable for studies of site-to-site or interdomain motions in proteins. In the case of labeled proteins we observed rapid diffusion of the D-A pair over a limited range of distances, which we interpreted as due to motions of the probes tethered by flexible linker such as lysine side chains [28]. In these cases it is difficult to imagine how one could resolve the slower interdomain motions. If a shorter lifetime is used to reveal the rate of the faster motions, then the inter-domain motions will not be observed. Conversely, if the donor lifetime is longer so as to reveal domain-to-domain motions, then the faster motions will not be resolved. This dilemma could be solved by labeling the protein with both a short- and a long-lived donor, thereby allowing resolution of both the faster and the slower D-A motions.

ACKNOWLEDGMENTS

REFERENCES

1. J. A. McCammon and S. C. Harvey (1987) *Dynamics of Proteins and Nucleic Acids,* Cambridge University Press, New York.
2. G. R. Welch (1986) *The Fluctuating Enzyme,* J. Wiley & Sons, New York.
3. J. R. Lakowicz, I. Gryczynski, H. Szmacinski, H. Cherek, and N. Joshi (1991) *Eur. Biophys. J.* **19**, 125.
4. J. R. Lakowicz, I. Gryczynski, J. Kuśba, and E. Danielsen (1992) *J. Fluoresc.* **2**, 247–258.
5. R. F. Steiner (1991) in J. R. Lakowicz (Ed.), *Topics in Fluorescence Spectroscopy. Vol. 2: Principles,* Plenum Press, New York, pp. 1–52.
6. T. Förster (1948) *Ann. Phys. (Leipzig)* **2**, 55–75.
7. L. Stryer (1978) *Annu. Rev. Biochem.* **47**, 819–846.
8. T. G. Dewey (1991) in T. G. Dewey (Ed.), *Biophysical and Biochemical Aspects of Fluorescence Spectroscopy,* Plenum Press, New York, p. 197.
9. C. R. Cantor and P. Pechukas (1971) *Proc. Natl. Acad. Sci. USA* **68**, 2099–2103.
10. E. Haas, M. Wilchek, E. Katchalski-Katzir, and I. Z. Steinberg (1975) *Proc. Natl. Acad. Sci. USA* **72**, 1807–1811.
11. J. R. Lakowicz, M. L. Johnson, W. Wiczk, A. Bhat, and R. F. Steiner (1987) *Chem. Phys. Lett.* **138**, 587–593.
12. E. Haas and I. Z. Steinberg (1984) *Biophys. J.* **46**, 429–437.
13. J. R. Lakowicz, J. Kuśba, W. Wiczk, I. Gryczynski, H. Szmacinski, and M. L. Johnson (1991) *Biophys. Chem.* **39**, 79–84.
14. J. M. Beechem and E. Haas (1989) *Biophys.* **49**, 1225–1236.
15. B. P. Maliwal, J. R. Lakowicz, G. Kupryszewski, and P. Rekowski (1993) *Biochemistry* **32**, 12337–12345.
16. J. M. Beechem, J. R. Knutson, J. B. A. Ross, B. W. Turner, and L. Brand (1983) *Biochemistry* **22**, 6054–6058.
17. J. R. Lakowicz, J. Kuśba, W. Wiczk, I. Gryczynski, and M. L. Johnson (1990) *Chem. Phys. Lett.* **173**, 319–326.
18. J. R. Lakowicz, J. Kuśba, I. Gryczynski, W. Wiczk, H. Szmacinski, and M. L. Johnson (1991) *J. Phys. Chem.* **95**, 9654–9660.
19. J. R. Lakowicz, J. Kuśba, H. Szmacinski, I. Gryczynski, P. Eis, W. Wiczk, and M. L. Johnson (1991) *Biopolymers* **31**, 1363–1378.
20. B. P. Maliwal, J. Kuśba, W. Wiczk, M. L. Johnson, and J. R. Lakowicz (1993) *Biophys. Chem.* **46**, 273–281.
21. G. Laczko, J. R. Lakowicz, I. Gryczynski, Z. Gryczynski, and H. Malak (1990) *Rev Sci. Instrum.* **61**, 2331–2337.
22. J. R. Lakowicz, W. Wiczk, I. Gryczynski, M. Fishman, and M. L. Johnson (1993) *Macromolecules* **26**, 349–363.
23. J. R. Lakowicz, J. Kuśba, W. Wiczk, I. Gryczynski, H. Szmacinski, and M. L. Johnson (1991) *Biophys. Chem.* **39**, 79–84.
24. M. L. Johnson and S. G. Frasier (1985) in S. N. Timasheff and C. H. W. Hirs (Eds.), *Methods in Enzymology 117,* Academic Press, New York, pp. 301–342.
25. J. R. Lakowicz, W. Wiczk, I. Gryczynski, H. Szmacinski, and M. L. Johnson (1990) *Biophys. Chem.* **38**, 99–109.
26. J. R. Lakowicz, H. Szmacinski, I. Gryczynski, W. Wiczk, and M. L. Johnson (1990) *J. Phys. Chem.* **94**, 8413–8416.
27. U. Gösele, M. Hauser, U. K. A. Kelin, and R. Frey (1975) *Chem. Phys. Lett.* **34**, 519–522.
28. J. R. Lakowicz, I. Gryczynski, J. Kuśba, W. Wiczk, H. Szmacinski, and M. L. Johnson (1993) *Photochem. Photobiol.* **59**(1), 16–29.